Engineering the spin conversion in graphene monolayer epitaxial structures

Cite as: APL Mater. 9, 061113 (2021); doi: 10.1063/5.0048612
Submitted: 24 February 2021 • Accepted: 3 June 2021 •
Published Online: 23 June 2021

Alberto Anadón,[1,a)] Adrián Gudín,[1] Rubén Guerrero,[1] Iciar Arnay,[1] Alejandra Guedeja-Marron,[1,2] Pilar Jiménez-Cavero,[3,4] Jose Manuel Díez Toledano,[1,5] Fernando Ajejas,[1,b)] María Varela,[6] Sebastien Petit-Watelot,[7] Irene Lucas,[3,4] Luis Morellón,[3,4] Pedro Antonio Algarabel,[3,4] Manuel Ricardo Ibarra,[3,4,8] Rodolfo Miranda,[1,5,9] Julio Camarero,[1,5,9] Juan Carlos Rojas-Sánchez,[7] and Paolo Perna[1,c)]

AFFILIATIONS

[1] IMDEA Nanociencia, C/Faraday 9, 28049 Madrid, Spain
[2] Departamento de Física de Materiales and Instituto Pluridisciplinar, Universidad Complutense de Madrid, Ciudad Universitaria, 28040 Madrid, Spain
[3] Instituto de Nanociencia y Materiales de Aragón, Universidad de Zaragoza and Consejo Superior de Investigaciones Científicas, 50018 Zaragoza, Spain
[4] Departamento de Física de la Materia Condensada, Universidad de Zaragoza, 50009 Zaragoza, Spain
[5] Departamento de Física de la Materia Condensada and Departamento de Física Aplicada and Instituto Nicolás Cabrera, Universidad Autónoma de Madrid, 28049 Madrid, Spain
[6] Departamento de Física de Materiales and Instituto Pluridisciplinar, Universidad Complutense de Madrid, 28040 Madrid, Spain
[7] Université de Lorraine, CNRS, IJL, Nancy, France
[8] Laboratorio de Microscopías Avanzadas, Universidad de Zaragoza, 50018 Zaragoza, Spain
[9] IFIMAC, Universidad Autónoma de Madrid, 28049 Madrid, Spain

Note: This paper is part of the Special Topic on Emerging Materials for Spin–Charge Interconversion.
[a)] **Author to whom correspondence should be addressed:** alberto.anadon@univ-lorraine.fr
[b)] **Current address:** Unité Mixte de Physique, CNRS, Thales, Univ. Paris-Sud, Université Paris-Saclay, Palaiseau, France.
[c)] **Electronic mail:** paolo.perna@imdea.org

ABSTRACT

Spin Hall and Rashba–Edelstein effects, which are spin-to-charge conversion phenomena due to spin–orbit coupling (SOC), are attracting increasing interest as pathways to manage rapidly and at low consumption cost the storage and processing of a large amount of data in spintronic devices as well as more efficient energy harvesting by spin-caloritronics devices. Materials with large SOC, such as heavy metals (HMs), are traditionally employed to get large spin-to-charge conversion. More recently, the use of graphene (gr) in proximity with large SOC layers has been proposed as an efficient and tunable spin transport channel. Here, we explore the role of a graphene monolayer between Co and a HM and its interfacial spin transport properties by means of thermo-spin measurements. The gr/HM (Pt and Ta) stacks have been prepared on epitaxial Ir(111)/Co(111) structures grown on sapphire crystals, in which the spin detector (i.e., top HM) and the spin injector (i.e., Co) are all grown *in situ* under controlled conditions and present clean and sharp interfaces. We find that a gr monolayer retains the spin current injected into the HM from the bottom Co layer. This has been observed by detecting a net reduction in the sum of the spin Seebeck and interfacial contributions due to the presence of gr and independent from the spin Hall angle sign of the HM used.

Spin–charge current interconversion based on spin–orbit coupling is an essential operation in present spintronics applications.[1–6] Systems showing these properties are promising candidates for the realization, for instance, of a new generation of nonvolatile magnetic random access memories or efficient energy harvesting devices,[7–9] among other examples. The most widespread systems providing large spin Hall conversion efficiency toward these applications are based on heavy metals, e.g., Pt, Ta, or W, because of their strong spin–orbit coupling (SOC).

Recently, two-dimensional (2D) materials, such as Rashba interfaces,[10,11] topological insulator surfaces,[12–14] and transition metal dichalcogenides,[15–24] have been proposed to obtain efficient spin–charge current interconversion[25] and their wide range of functional properties. Some can present large SOC,[15,17,19,26] while others such as gr can exhibit micrometer spin diffusion lengths and long spin lifetimes.[27] In addition, the properties of gr can be tuned by proximity with other materials, such as ferromagnets (FMs),[28,29] heavy metals,[30] or even other 2D materials.[17]

In this regard, it has been observed recently that the gr/Pt interface presents a very high spin-to-charge output voltage at room temperature (RT) in lateral spin valve devices using exfoliated gr and electrodes grown *ex situ* by electron beam lithography.[31,32] The enhanced spin–charge signal was due to the combination of current shunting suppression, highly resistive platinum, and efficient spin injection into gr. However, in contrast, it has also been observed that gr can significantly reduce the spin pumping voltage[33,34] or even generate a spin pumping voltage by itself without the necessity of a HM due to interfacial spin–orbit interactions.[35,36] These discrepancies, together with the low intrinsic SOC of gr, point toward the relevance of the quality of the interfaces in determining the overall spin transport properties.

Here, we study the interface between the gr monolayer and a HM and its effect on spin-to-charge current conversion in epitaxial systems in which the spin detector (i.e., top HM), the gr layer, and the spin injector (i.e., Co) are all grown *in situ* under controlled conditions and with clean and sharp interfaces. All the samples have an (111)Ir 10 nm buffer layer and a 1.6 nm-thick Co layer on top of it. Then, we have two different types of stacks on top of the Ir/Co: gr/HM and HM. The role of gr in determining the overall spin-to-charge current conversion has been disentangled by means of thermo-spin experiments, as shown in Fig. 1. In these experiments, which are done in the so-called longitudinal spin Seebeck effect (SSE) configuration,[8,37] the SSE and the anomalous Nernst effect (ANE)[38] coexist in this geometry. In order to separate both contributions, we first use an Ir/Co/Ir control sample to obtain the ANE in the Co layer. We subtract this contribution in all the other heterostructures in order to obtain the overall spin–charge current contribution. We demonstrate that the spin–charge conversion in a Co/gr/HM system is not enhanced compared to the reference Co/HM and independent from the spin Hall angle sign of the HM used as spin detectors, i.e., Pt or Ta. This experimental finding highlights the importance of gr to engineer the spin conversion and for the development of spin-caloritronics and spin-orbitronics devices.

The samples incorporating gr (i.e., gr/HM) and the ones without gr (i.e., HM) were all fabricated *in situ* on epitaxial Ir(111)/Co(111) grown on sapphire crystals under controlled conditions, that is, they present similar structural quality and clean

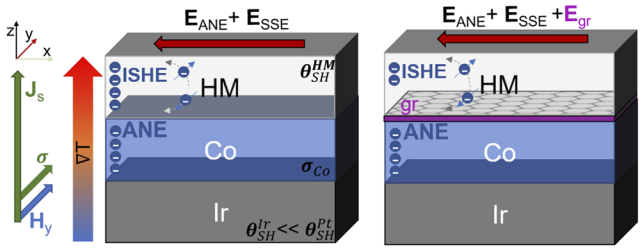

FIG. 1. Schematic of thermo-spin measurements in graphene metal hybrid heterostructures. When a thermal gradient is applied in an Ir/Co/Pt structure in the z direction as well as a magnetic field in the y direction, a spin current ($\mathbf{J_s}$) is generated in the z direction and we will observe two different thermo-spin contributions, the anomalous Nernst effect ($\mathbf{E_{ANE}}$) and the spin Seebeck effect ($\mathbf{E_{SSE}}$). When a graphene monolayer is introduced, we will need to consider not only the effect of graphene itself but also the additional contributions of the two new interfaces in the system ($\mathbf{E_{gr}}$), which may induce the inverse Rashba–Edelstein effect as well as spin memory loss, a partial loss of spin current coherence.

interfaces. We followed the methodology described in Refs. 28 and 39. In brief, we first deposited a 10 nm-thick epitaxial Ir(111) on Al_2O_3(0001) single crystal substrates by DC sputtering at 670 K with a partial Ar pressure of $8 \cdot 10^{-3}$ mbar and low deposition rate (of 0.3 Å/s). Subsequently, in the case of the gr-based heterostructures, the monolayer gr was prepared by chemical vapor deposition by ethylene dissociation at 1025 K at a partial pressure of $5.5 \cdot 10^{-6}$ mbar. The samples were then cooled down to RT and Co was deposited by molecular beam epitaxy, and then, the Co intercalation below gr was promoted by thermal annealing at 550 K. This procedure produces the formation of a homogeneous Co layer with high structural order and sharp interfaces.[28,39] The Co layer is monitored in every step of the growth by x-ray photoemission spectroscopy to assure that it is not oxidized. In the case of samples without gr, we deposited a 1.6 nm-thick Co layer by DC sputtering at RT on top of the Ir(111) buffer. Finally, in all samples, a 5 nm capping layer of Pt or Ta was DC sputtered at RT.

To prove the structural quality of the samples, we resorted to x-ray diffraction (XRD) and high resolution scanning transmission electron measurements (STEMs) at RT. The XRD measurements were performed using a commercial Rigaku SmartLab SE multipurpose diffractometer with a monochromatic Cu Kα source (λ = 1.54 Å). STEM observations were carried out in a JEOL ARM200cF at 200 kV and RT. The microscope is equipped with a CEOS spherical aberration corrector and a Gatan Quantum electron energy-loss spectrometer.[28] Specimens were prepared by mechanical polishing and Ar ion milling.

Figure 2(a) shows a θ–2θ diffraction pattern recorded in a Al_2O_3//Ir/Co/gr/Ta heterostructure. Besides the Al_2O_3[0006] and Al_2O_3[00012] crystallographic reflections from the substrate, maximum intensity appears at 2θ = 40.6° and 87.9°, which corresponds with Ir[111] and Ir[222] reflections, respectively. The formation of thickness fringes around the Ir[111] and Ir[222] reflections confirms the low roughness of the interfaces. In the inset, the ω scan (rocking curve) around the Ir[222] reflection shows a sharp profile. The curve was fitted using a pseudo-voigt function obtaining a full width at half maximum (FWHM) of 0.27°, which proves a low degree of mosaicity in the deposited films. Figure 2(b) shows φ scans

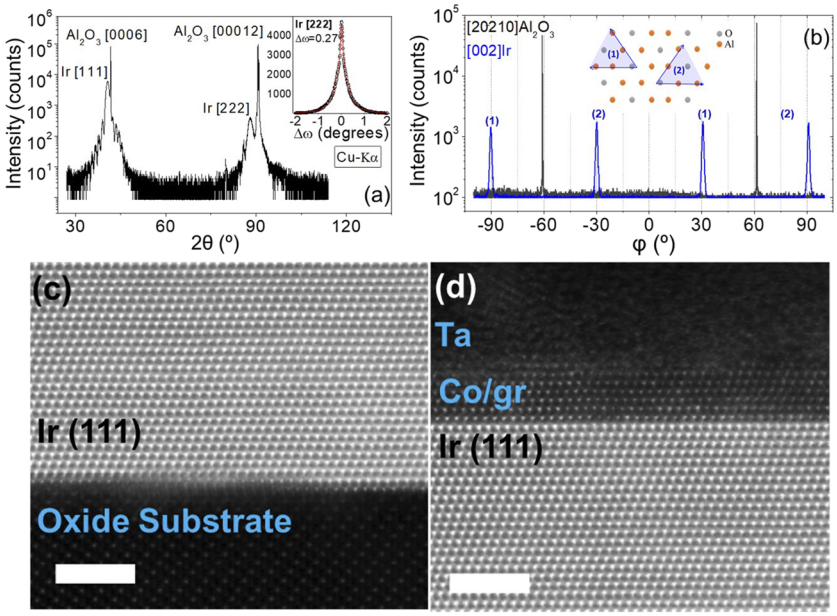

FIG. 2. Structural and microscopic characterization of epitaxial Ir/Co/gr/HM heterostructures. (a) X-ray θ–2θ diffraction pattern recorded in an Al_2O_3//Ir/Co/gr heterostructure. In the inset, a θ–2θ scan recorded around the Ir(111) reflection is shown. (b) φ scan plots of the Al_2O_3[20–210] and Ir[002] reflections. (c) and (d) Scanning transmission electron microscopy characterization of a Ir[111]/Co/gr sample grown on a $SrTiO_3$ substrate (with t_{Co} = 1 nm and t_{Ir} = 10 nm), capped with a Ta oxide thick layer in order to protect the gr surface. Atomic resolution high-angle annular dark-field images of the STO/Ir and Ir/Co interfaces, respectively. The scale bars represent a length of 2 nm.

around the $Al_2O_3[202 \cdot \bar{1}10]$ and Ir[002] reflections. The rotation scan around the Ir[002] reflection shows a sixfold symmetry instead of the expected threefold symmetry. This is related with the presence of two equivalent twin-boundary domains rotated by 180°.[40] Similar curves, including ω- and φ-scans, are obtained for samples without gr (not shown). From Figs. 2(a) and 2(b), the following epitaxial relations are obtained: out-of-plane $[0001]Al_2O_3 \| [111]$Ir and two in-plane configurations, (1) $[01\text{–}10]Al_2O_3 \| [1\text{–}10]$Ir (−90° and 30°) and (2) $[01\text{–}10]Al_2O_3 \| [1\text{–}10]$Ir (30° and 90°). The positions of the Ir[111] and Ir[002] reflections indicate an incommensurate growth of iridium with a bulk-like afcc lattice parameter within the experimental error. This is explained by the large mismatch (~13%) between Al_2O_3[0001] (0.4785 nm) and Ir[111].

The STEM observations confirm the quality of the stacks. Figures 2(c) and 2(d) display the atomic resolution STEM high-angle dark-field image of an Ir/Co/gr/Ta heterostructure, showing a high crystalline quality and sharp and coherent interface. No major hints of chemical interdiffusion or disorder are visible. These results, along with x-ray diffraction, suggest that the Co layer is epitaxial and the Co layer on the Ir buffer is fully strained and coherent.

Thermo-spin measurements were performed in an Oxford spectrostat NMR40 continuous flow He cryostat with a thermoelectric measurement system.[41–43] Experimentally, the sample is put in place between two ceramic AlN plates, which are electrically insulating but have high thermal conductivity. They are attached using thermal paste to a large Cu piece that acts as a cold feet and is in direct contact with the cryostat. A resistive heater on the upper AlN piece provides the thermal gradient by application of an electric current in the order of several milliamperes. The temperature difference between the upper and lower plate is measured by two T-type thermocouples near to the sample in order to obtain accurate temperature values. The samples were contacted electrically with thin Al wires with a diameter of 25 μm using commercial thermal silver paste. The voltage was measured using a Keithley 2182A nanovoltmeter. The sketch of the measurement geometry is shown in Fig. 1: the thermal gradient is applied in the z direction, while a magnetic field is swept in the y direction. A thermo-spin voltage is then measured in the x direction.

It is worth recalling that in systems containing metallic FMs, the thermo-spin voltage has three main contributions: (1) the anomalous Nernst effect (ANE), i.e., the thermal counterpart of the anomalous Hall effect, which has a similar physical origin;[8,38,43] (2) the spin Seebeck effect, which comprises the generation of a spin current from incoherent thermal excitation and its conversion on an electric voltage by means of the inverse spin Hall effect (ISHE); and (3) the interfacial spin–orbit contribution, arising from the Rashba interfacial spin–orbit field, which can give rise to a wide range of phenomena, from spin memory loss to spin current generation.[6,10,44]

We first identified the ANE signal contribution of the Co layer, which is proportional to the Co magnetization. We acquired the thermo-spin voltage in a symmetric epitaxial Ir(10)/Co(1.6)/Ir(5) stack [panel (b)] as a function of the in-plane applied magnetic field and compared it to the sample magnetization along the y direction normalized by the saturation value. The identical behavior of both magnitudes is shown in Fig. 3(b), as expected from the ANE phenomenological relation

$$\mathbf{E_{ANE}} = Q_S(\mu_0 \mathbf{M} \times \nabla T), \tag{1}$$

with Q_S, μ_0, $\mathbf{M}$, and ∇T being the Nernst coefficient, the vacuum magnetic permeability, the thermal gradient, and the magnetization of the FM, respectively.

Since Ir has a much smaller spin Hall than other heavy metals, such as Pt,[45] this symmetric stack can be hence used as a reference to check the size of the anomalous Nernst effect of the Co layer in the asymmetric stacks, which will be subtracted from the overall voltage measured. Note that in Figs. 3(a) and 3(b), we can observe a very

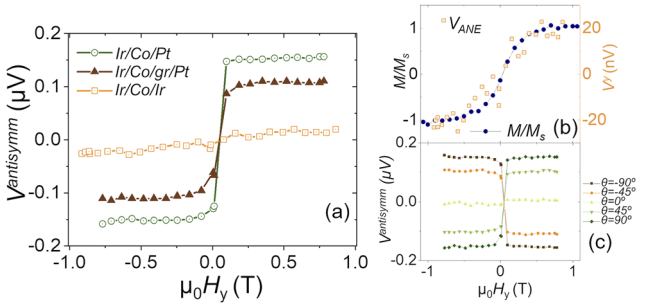

FIG. 3. Thermo-spin voltage in epitaxial hybrid gr/HM and HM stacks. (a) Thermo-spin voltage in Ir/Co/Ir, Ir/Co/Pt, and Ir/Co/gr/Pt. The observed thermo-spin voltage in the sample with the Ir capping layer (yellow) is significantly smaller than the that with Pt, and it is mainly due to the anomalous Nernst effect in Co. A reduction in the voltage at saturation field is observed when gr is introduced into the stack. (b) Close-up view on the anomalous Nerst effect voltage in the Ir/Co/Ir sample and its magnetization measured by vibrating sample magnetometry. (c) Angular dependence on the thermo-spin voltage in the Ir/Co/Pt sample. The angle θ represents the relative angle between the measured voltage (x direction) and the applied magnetic field (xy plane).

small voltage in the Co/Ir sample mainly due to the electrical screening by the buffer layer of Ir because of its low resistivity, about three times lower than Pt in this range of thickness.[46–48] This is specially the case for epitaxial Ir,[49] which leads to smaller values of the spin Hall angle when comparing to polycrystalline metals (see Ref. 48).

The second contribution to the measured voltage is the SSE generated by the inverse spin Hall effect,[50,51] which has a similar geometric behavior, since the spin current lies in the z direction as it is induced by an out-of-plane thermal gradient,

$$\mathbf{J_C} = \frac{\theta_{SH}\rho}{A}\left(\frac{2e}{\hbar}\right)\mathbf{J_S} \times \boldsymbol{\sigma}, \tag{2}$$

where $\mathbf{J_C}$ and $\mathbf{J_s}$ are the charge and spin currents in the HM, respectively, θ_{SH} and ρ are the spin Hall angle and the electrical resistivity of the HM, respectively, A represents the contact area between the FM and the HM, e is the elementary charge, and $\boldsymbol{\sigma}$ is the mean spin polarization direction of the electrons in the FM close to the interface with the HM. It is important to note here that $\mathbf{J_S} \propto \nabla T$ and $\boldsymbol{\sigma} \propto \mathbf{M}$ in the FM at saturation.

We have thus performed thermo-spin measurements in the Pt and gr/Pt samples. This is shown in Fig. 3(a) where we observe that the introduction of gr reduces the total observed thermo-spin voltage in the Ir/Co/Pt system by about 40%.

As can be seen in Eqs. (1) and (2), the SSE and ANE voltages follow a cross product relation between the thermal gradient and the magnetization; therefore, when magnetization rotates in the xy plane and the x component of the thermo-spin electric field is measured, we will observe a sinusoidal relation, as shown in Fig. 3(c), where the angle θ represents the relative angle between the measured voltage and the applied magnetic field.

At this point, it is important to notice that (i) the dependence of the thermo-spin voltage with an external magnetic field is similar for both effects and (ii) the comparison of thermal gradients in Co in these stacks is reliable. For the latter, we routinely checked that the total thermal conductivity of the system, i.e., the sample (mainly substrate) with its holder, is maintained unchanged in all experiments and all samples. In fact, the main contributions to the thermal resistance of the system come from the substrate and sample holder because their total thermal resistance is orders of magnitude larger than that of the thin film stack. Consequently, the heat current that flows through Co, which has the same thickness in all samples, is similar in all the cases. This implies that the inclusion of gr or different metallic detecting layers does not modify the (perpendicular) thermal gradient in Co and that the corresponding spin current is kept reasonably unchanged for all samples.

As remarked before, the ANE signal of the Co layer taken from the measurements of the symmetric Ir/Co/Ir system is subtracted from the voltages acquired in the asymmetric stacks with the Pt detecting layer with and without gr. We carefully considered the resistivities and thickness of the films in the system. This is shown in the supplementary material. Thus, the ANE (V_{ANE}^{contr}) contribution to the voltage in the x direction for a multilayer system can be estimated for each sample as[42,51]

$$V_{ANE}^{contr} = \left(\frac{r}{1+r}\right)V_{ANE}, \tag{3}$$

where V_{ANE} is the anomalous Nernst effect voltage of a single metallic FM layer with the same thickness subjected to the same thermal gradient and $r = \frac{\rho_{HM}}{\rho_{FM}}\frac{t_{FM}}{t_{HM}}$, with ρ_{HM} and ρ_{FM} representing the HM and Co resistivities and t_{HM} and t_{FM} representing their thickness, respectively.

The resulting voltage dependences on the applied magnetic field after subtraction of the ANE contribution are shown in Fig. 4. Here, the voltage signals are normalized by the sample resistance to rule out the possibility of a shunting effect in the gr monolayer in the inverse spin Hall signal. We also assume for this calculation that

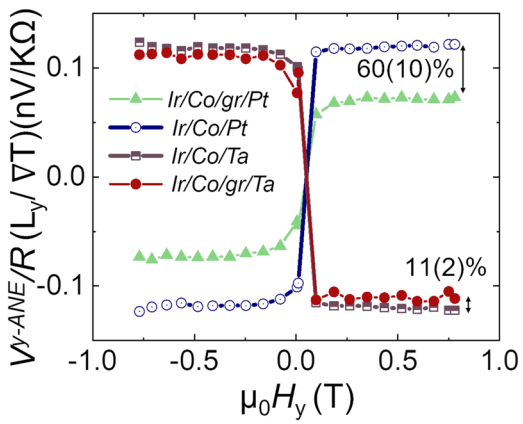

FIG. 4. Interfacial contribution to the thermo-spin voltage. (a) Thermo-spin voltage after subtraction of the anomalous Nernst effect component. This value is divided by the sample resistance in order to reduce artifacts and compare the values adequately. L_x = 0.8 mm represents the lateral dimension of the sample in the x direction and $\nabla T = (T_{hot} - T_{cold})/L_z$, where L_z = 0.4 mm is the sample thickness, including the substrate. The absolute saturation voltage observed in the Pt sample (blue open circles) is reduced by 60% when comparing with the gr/Pt sample (green triangles). This is also the case for the absolute voltage in the Ta sample (wine squares) compared to gr/Ta (red filled circles) where the observed reduction is 11%.

Ms is the same in all the samples. To break down the contribution of the gr monolayer, in addition to the gr/Pt- and Pt-based stacks, we have considered a second set of samples capped by a 5 nm-thick Ta layer with a naturally oxidized surface (i.e., gr/Ta- and Ta-based stacks). As clearly shown in Fig. 4, the voltage dependence with the external magnetic field has an opposite sign when comparing Ta and Pt samples, as expected from their different signs of the spin Hall angle. Although the signal reductions in the two types of samples are of different magnitudes, that is, 60% in Pt-based samples and 11% in the Ta-based samples, our experimental finding suggests a universal behavior regardless of the detecting layer. Here, the reduction percentage is calculated by subtracting the voltage at $\mu_0 H = 0.7$ T as $|(V_{HM} - V_{gr/HM})/V_{gr/HM} \cdot 100|$.

There are different mechanisms that may be behind the origin of this observation. In this experiment, gr may support a non-negligible SOC, induced by the adjacent metals through electronic hybridization. This, in turn, produces a significant Rashba-type Dzyaloshinskii–Moriya interaction (DMI).[28,29,40] On this basis, we envisage three different mechanisms responsible for the reduction of the measured thermo-spin signals. (i) The introduction of gr could produce a shunting of the ISHE current, reducing the effective spin-to-charge conversion in the HM. This artifact is avoided normalizing the thermo-spin voltages by the sample resistance, as shown in Fig. 4. (ii) A Rashba interface, such as the Co/gr in our system, can induce spin–charge conversion by the so-called inverse Rashba–Edelstein effect (IREE). This would be translated in a voltage contribution of similar sign and magnitude for both systems. As we observe, this scenario cannot explain our findings unless the hybridization of gr due to the HM changes substantially the effective IREE of the interface. The IREE has already been observed in YIG/gr by spin pumping,[35,36] and after normalization by sample resistance, its magnitude is significantly smaller than the ISHE in Pt, although it could be different in the case of Co/gr. (iii) The gr interfaces are characterized by the presence of an interfacial spin–orbit coupling field that can affect the spin coherence,[6,46,52–54] depolarizing the spin current traveling across it and thus reducing the total observed signal. This effect, referred to as spin memory loss (SML), may happen in both Co/gr[28] and gr/HM[46] interfaces. The fact that the reduction is smaller in the case of Ta could be explained by its smaller SML when compared to Pt interfaces.[6,55] Another plausible scenario could also arise considering a combination of the IREE effect and SML. In summary, we may have a different enhancement or attenuation depending on the nature of the HM. In addition, even though saturation magnetization can play an important role in ANE measurements,[42,56] this interpretation still holds even if the value of the saturation magnetization (Ms) is significantly different in both systems. As shown in the supplementary material, we obtain a higher average Ms in the gr samples, suggesting that the thermo-spin voltage suppression by graphene could be even larger than the estimation that we provide in Fig. 4. Further experiments including the direct injection of spin current are necessary in order to discern between both contributions since while spin Hall and inverse spin Hall are reciprocal effects, this is not necessarily the case of the Rashba–Edelstein effect and its inverse counterpart.

Summarizing, we have fabricated high quality epitaxial hybrid metallic/monolayer graphene stacks with coherent, roughness-free interfaces as confirmed by x-ray diffraction and atomically resolved scanning transmission electron microscopy experiments. We have explored the spin–charge conversion by means of thermo-spin measurements in which we have carefully disentangled the anomalous Nernst effect from the spin Seebeck and interfacial contributions. Furthermore, we estimated the interfacial contribution when a graphene monolayer is inserted. Although in other experiments the gr/Pt system has been shown to increase the spin Hall effect efficiency, we demonstrate that, for thermally induced spin currents in the longitudinal spin Seebeck configuration, the presence of graphene reduces the overall spin–charge conversion regardless of the heavy metal (Ta or Pt with different spin Hall angle signs) layer used. We disregard any possible effect of the introduction of graphene in the thermal gradient in Co due to the insignificant change that the thermal resistance of graphene introduces in the system compared to the total thermal resistance of the sample and sample holder. We ascribe the reduction in the thermo-spin voltage mainly to the combination of spin memory loss and the inverse Rashba–Edelstein effect.

See the supplementary material for more information on the anomalous Nernst effect contribution in thermo-spin measurements and the saturation magnetization in ultra-thin cobalt films.

We thank V. P. Amin, S. Sangiao, A. Fert, and F. Casanova for valuable discussions. This research was supported by the Regional Government of Madrid through Project No. P2018/NMT-4321 (NANOMAGCOST-CM) and the Spanish Ministry of Economy and Competitiveness (MINECO) through Project Nos. RTI2018-097895-B-C42, RTI2018-097895-B-C43 (FUN-SOC), PGC2018-098613-B-C21 (SpOrQuMat), PGC2018-098265-B-C31, and PCI2019-111867-2 (FLAG ERA 3 grant SOgraphMEM). J.M.D.T. and A.G. acknowledge support from MINECO and CM through Grant Nos. BES-2017-080617 and PEJD-2017-PREIND-4690, respectively. I.A. acknowledges financial support from the Regional Government of Madrid through Contract No. PEJD-2019-POST/IND-15343. IMDEA Nanoscience is supported by the "Severo Ochoa" Program for Centres of Excellence in R&D, MINECO (Grant No. SEV-2016-0686). A.A., S.P.-W., and J.-C.R.-S. acknowledge support from Toptronic ANR through Project No. ANR-19-CE24-0016-01. P.J.-C., I.L., L.M., P.A.A., and M.R.I. acknowledge support from Project No. MAT2017-82970-C2-R. Electron microscopy observations were carried out at the Centro Nacional de Microscopía Electrónica at the Universidad Complutense de Madrid.

DATA AVAILABILITY

The data that support the findings of this study are available from the corresponding author upon reasonable request.

REFERENCES

[1] I. M. Miron, K. Garello, G. Gaudin, P.-J. Zermatten, M. V. Costache, S. Auffret, S. Bandiera, B. Rodmacq, A. Schuhl, and P. Gambardella, Nature **476**, 189 (2011).

[2] X. Fan, H. Celik, J. Wu, C. Ni, K.-J. Lee, V. O. Lorenz, and J. Q. Xiao, Nat. Commun. **5**, 3042 (2014).

[3] K. Jhuria, J. Hohlfeld, A. Pattabi, E. Martin, A. Y. A. Córdova, X. Shi, R. L. Conte, S. Petit-Watelot, J. C. Rojas-Sanchez, G. Malinowski *et al.*, Nat. Electron. **3**, 680 (2020).

[4]K. Garello, I. M. Miron, C. O. Avci, F. Freimuth, Y. Mokrousov, S. Blügel, S. Auffret, O. Boulle, G. Gaudin, and P. Gambardella, Nat. Nanotechnol. **8**, 587 (2013).
[5]J. Kim, J. Sinha, M. Hayashi, M. Yamanouchi, S. Fukami, T. Suzuki, S. Mitani, and H. Ohno, Nat. Mater. **12**, 240 (2013); arXiv:1207.2521.
[6]A. Anadón, R. Guerrero, J. A. Jover-Galtier, A. Gudín, J. M. Díez Toledano, P. Olleros-Rodríguez, R. Miranda, J. Camarero, and P. Perna, ACS Appl. Nano Mater. **4**, 487 (2021).
[7]G. E. W. Bauer, E. Saitoh, and B. J. van Wees, Nat. Mater. **11**, 391 (2012).
[8]K. Uchida, M. Ishida, T. Kikkawa, A. Kirihara, T. Murakami, and E. Saitoh, J. Phys.: Condens. Matter **26**, 343202 (2014).
[9]R. Ramos, A. Anadón, I. Lucas, K. Uchida, P. A. Algarabel, L. Morellón, M. H. Aguirre, E. Saitoh, and M. R. Ibarra, APL Mater. **4**, 104802 (2016); arXiv:1605.03752.
[10]J. C. Sánchez, L. Vila, G. Desfonds, S. Gambarelli, J. P. Attané, J. M. De Teresa, C. Magén, and A. Fert, Nat. Commun. **4**, 2944 (2013).
[11]A. D. Caviglia, M. Gabay, S. Gariglio, N. Reyren, C. Cancellieri, and J.-M. Triscone, Phys. Rev. Lett. **104**, 126803 (2010).
[12]J.-C. Rojas-Sánchez, S. Oyarzún, Y. Fu, A. Marty, C. Vergnaud, S. Gambarelli, L. Vila, M. Jamet, Y. Ohtsubo, A. Taleb-Ibrahimi, P. Le Fèvre, F. Bertran, N. Reyren, J.-M. George, and A. Fert, Phys. Rev. Lett. **116**, 096602 (2016).
[13]A. R. Mellnik, J. S. Lee, A. Richardella, J. L. Grab, P. J. Mintun, M. H. Fischer, A. Vaezi, A. Manchon, E.-A. Kim, N. Samarth *et al.*, Nature **511**, 449 (2014).
[14]Y. Fan, X. Kou, P. Upadhyaya, Q. Shao, L. Pan, M. Lang, X. Che, J. Tang, M. Montazeri, K. Murata *et al.*, Nat. Nanotechnol. **11**, 352 (2016).
[15]W.-Y. Lee, N.-W. Park, G.-S. Kim, M.-S. Kang, J. W. Choi, K.-Y. Choi, H. W. Jang, E. Saitoh, and S.-K. Lee, Nano Lett. **21**, 189 (2020).
[16]W. Lv, Z. Jia, B. Wang, Y. Lu, X. Luo, B. Zhang, Z. Zeng, and Z. Liu, ACS Appl. Mater. Interfaces **10**, 2843 (2018).
[17]L. A. Benítez, W. Savero Torres, J. F. Sierra, M. Timmermans, J. H. Garcia, S. Roche, M. V. Costache, and S. O. Valenzuela, Nat. Mater. **19**, 170 (2020); arXiv:1908.07868.
[18]X. Lin, W. Yang, K. L. Wang, and W. Zhao, Nature Electronics **2**, 274–283 (2019).
[19]P. Debashis, T. Y. Hung, and Z. Chen, npj 2D Mater. Appl. **4**, 18 (2020).
[20]G. M. Stiehl, D. MacNeill, N. Sivadas, I. El Baggari, M. H. Guimarães, N. D. Reynolds, L. F. Kourkoutis, C. J. Fennie, R. A. Buhrman, and D. C. Ralph, ACS Nano **13**, 2599 (2019); arXiv:1901.08908.
[21]M. H. D. Guimarães, G. M. Stiehl, D. MacNeill, N. D. Reynolds, and D. C. Ralph, Nano Lett. **18**, 1311 (2018); arXiv:1801.07281.
[22]D. MacNeill, G. M. Stiehl, M. H. D. Guimaraes, R. A. Buhrman, J. Park, and D. C. Ralph, Nat. Phys. **13**, 300 (2017); arXiv:1605.02712.
[23]D. Macneill, G. M. Stiehl, M. H. Guimarães, N. D. Reynolds, R. A. Buhrman, and D. C. Ralph, Phys. Rev. B **96**, 054450 (2017); arXiv:1707.03757.
[24]Q. Xie, W. Lin, B. Yang, X. Shu, S. Chen, L. Liu, X. Yu, M. B. H. Breese, T. Zhou, M. Yang, Z. Zhang, S. Wang, H. Yang, J. Chai, X. Han, and J. Chen, Adv. Mater. **31**, 1900776 (2019).
[25]J.-C. Rojas-Sánchez and A. Fert, Phys. Rev. Appl. **11**, 054049 (2019).
[26]F. Herling, C. K. Safeer, J. Ingla-Aynés, N. Ontoso, L. E. Hueso, and F. Casanova, APL Mater. **8**, 071103 (2020).
[27]S. Roche, J. Åkerman, B. Beschoten, J. C. Charlier, M. Chshiev, S. P. Dash, B. Dlubak, J. Fabian, A. Fert, M. Guimarães, F. Guinea, I. Grigorieva, C. Schönenberger, P. Seneor, C. Stampfer, S. O. Valenzuela, X. Waintal, and B. Van Wees, 2D Mater. **2**, 030202 (2015).
[28]F. Ajejas, A. Gudín, R. Guerrero, A. Anadón Barcelona, J. M. Diez, L. de Melo Costa, P. Olleros, M. A. Niño, S. Pizzini, J. Vogel, M. Valvidares, P. Gargiani, M. Cabero, M. Varela, J. Camarero, R. Miranda, and P. Perna, Nano Lett. **18**, 5364 (2018).
[29]H. Yang, G. Chen, A. A. C. Cotta, A. T. N'Diaye, S. A. Nikolaev, E. A. Soares, W. A. A. Macedo, K. Liu, A. K. Schmid, A. Fert, and M. Chshiev, Nat. Mater. **17**, 605 (2018).
[30]J. Balakrishnan, G. K. W. Koon, A. Avsar, Y. Ho, J. H. Lee, M. Jaiswal, S.-J. Baeck, J.-H. Ahn, A. Ferreira, M. A. Cazalilla, A. H. C. Neto, and B. Özyilmaz, Nat. Commun. **5**, 4748 (2014).
[31]W. Savero Torres, J. F. Sierra, L. A. Benítez, F. Bonell, M. V. Costache, and S. O. Valenzuela, 2D Mater. **4**, 041008 (2017).
[32]W. Yan, E. Sagasta, M. Ribeiro, Y. Niimi, L. E. Hueso, and F. Casanova, Nat. Commun. **8**, 661 (2017).
[33]M. Piquemal-Banci, R. Galceran, S. M.-M. Dubois, V. Zatko, M. Galbiati, F. Godel, M.-B. Martin, R. S. Weatherup, F. Petroff, A. Fert *et al.*, Nat. Commun. **11**, 5670 (2020).
[34]J. Park, I. Oh, A.-Y. Lee, H. Jang, J.-W. Yoo, Y. Jo, and S.-Y. Park, J. Alloys Compd. **829**, 154534 (2020).
[35]J. B. S. Mendes, O. Alves Santos, T. Chagas, R. Magalhães-Paniago, T. J. A. Mori, J. Holanda, L. M. Meireles, R. G. Lacerda, A. Azevedo, and S. M. Rezende, Phys. Rev. B **99**, 214446 (2019).
[36]J. B. S. Mendes, O. Alves Santos, L. M. Meireles, R. G. Lacerda, L. H. Vilela-Leão, F. L. A. Machado, R. L. Rodríguez-Suárez, A. Azevedo, and S. M. Rezende, Phys. Rev. Lett. **115**, 226601 (2015).
[37]S. M. Rezende, R. L. Rodríguez-Suárez, R. O. Cunha, A. R. Rodrigues, F. L. A. Machado, G. A. Fonseca Guerra, J. C. Lopez Ortiz, and A. Azevedo, Phys. Rev. B **89**, 014416 (2014).
[38]R. Ramos, M. H. Aguirre, A. Anadón, J. Blasco, I. Lucas, K. Uchida, P. A. Algarabel, L. Morellón, E. Saitoh, and M. R. Ibarra, Phys. Rev. B **90**, 054422 (2014).
[39]F. Ajejas, A. Anadon, A. Gudin, J. M. Diez, C. G. Ayani, P. Olleros-Rodríguez, L. De Melo Costa, C. Navio, A. Gutierrez, F. Calleja *et al.*, ACS Appl. Mater. Interfaces **12**, 4088 (2019).
[40]M. Blanco-Rey, P. Perna, A. Gudin, J. M. Diez, A. Anadón, P. Olleros-Rodríguez, L. de Melo Costa, M. Valvidares, P. Gargiani, A. Guedeja-Marron, M. Cabero, M. Varela, C. García-Fernández, M. M. Otrokov, J. Camarero, R. Miranda, A. Arnau, and J. I. Cerdá, ACS Appl. Nano Mater. **4**, 4398 (2021).
[41]R. Ramos, T. Kikkawa, M. H. Aguirre, I. Lucas, A. Anadon, T. Oyake, K. Uchida, H. Adachi, J. Shiomi, P. A. Algarabel, L. Morellon, S. Maekawa, E. Saitoh, and M. R. Ibarra, Phys. Rev. B **92**, 220407 (2015).
[42]A. Anadón, R. Ramos, I. Lucas, P. A. Algarabel, L. Morellón, M. R. Ibarra, and M. H. Aguirre, Appl. Phys. Lett. **109**, 012404 (2016).
[43]A. Sola, M. Kuepferling, V. Basso, M. Pasquale, T. Kikkawa, K. Uchida, and E. Saitoh, J. Appl. Phys. **117**, 17C510 (2015).
[44]V. P. Amin, J. Zemen, and M. D. Stiles, Phys. Rev. Lett. **121**, 136805 (2018); arXiv:1803.00593.
[45]T. Fache, J. C. Rojas-Sanchez, L. Badie, S. Mangin, and S. Petit-Watelot, Phys. Rev. B **102**, 064425 (2020).
[46]J.-C. Rojas-Sánchez, N. Reyren, P. Laczkowski, W. Savero, J.-P. Attané, C. Deranlot, M. Jamet, J.-M. George, L. Vila, and H. Jaffrès, Phys. Rev. Lett. **112**, 106602 (2013).
[47]G. K. Reeves, M. W. Lawn, and R. G. Elliman, J. Vac. Sci. Technol., A **10**, 3203 (1992).
[48]E. Sagasta, Y. Omori, M. Isasa, M. Gradhand, L. E. Hueso, Y. Niimi, Y. Otani, and F. Casanova, Phys. Rev. B **94**, 060412 (2016); arXiv:1603.04999.
[49]T. D. Khoa, S. Horii, and S. Horita, Thin Solid Films **419**, 88 (2002).
[50]M. B. Jungfleisch, A. V. Chumak, A. Kehlberger, V. Lauer, D. H. Kim, M. C. Onbasli, C. A. Ross, M. Kläui, and B. Hillebrands, Phys. Rev. B **91**, 134407 (2013); arXiv:1308.3787.
[51]R. Ramos, T. Kikkawa, K. Uchida, H. Adachi, I. Lucas, M. H. Aguirre, P. Algarabel, L. Morellón, S. Maekawa, E. Saitoh, and M. R. Ibarra, Appl. Phys. Lett. **102**, 072413 (2013).
[52]K. Dolui and B. K. Nikolić, Phys. Rev. B **96**, 220403 (2017).
[53]V. P. Amin and M. D. Stiles, Phys. Rev. B **94**, 104419 (2016); arXiv:1606.05758.
[54]V. P. Amin and M. D. Stiles, Phys. Rev. B **94**, 104420 (2016).
[55]S. N. Panda, S. Mondal, J. Sinha, S. Choudhury, and A. Barman, Sci. Adv. **5**, eaav7200 (2019).
[56]G. Venkat, C. D. W. Cox, D. Voneshen, A. J. Caruana, A. Piovano, M. D. Cropper, and K. Morrison, Phys. Rev. Mater. **4**, 075402 (2020).